

Stability Monitoring of Rotorcraft Systems: A Dynamic Data-Driven Approach

Siddharth Sonti

Mechanical Engineering Department,
Pennsylvania State University,
University Park, PA 16802
e-mail: sus39@psu.edu

Eric Keller

Mechanical Engineering Department,
Pennsylvania State University,
University Park, PA 16802
e-mail: keller.ee@gmail.com

Joseph Horn

Aerospace Engineering Department,
Pennsylvania State University,
University Park, PA 16802
e-mail: joehorn@psu.edu

Asok Ray

Fellow ASME
Mechanical Engineering Department,
Pennsylvania State University,
University Park, PA 16802
e-mail: axr2@psu.edu

This brief paper proposes a dynamic data-driven method for stability monitoring of rotorcraft systems, where the underlying concept is built upon the principles of symbolic dynamics. The stability monitoring algorithm involves wavelet-packet-based preprocessing to remove spurious disturbances and to improve the signal-to-noise ratio (SNR) of the sensor time series. A quantified measure, called Instability Measure, is constructed from the processed time series data to obtain an estimate of the relative instability of the dynamic modes of interest on the rotorcraft system. The efficacy of the proposed method has been established with numerical simulations where correlations between the instability measure and the damping parameter(s) of selected dynamic mode(s) of the rotor blade are established. [DOI: 10.1115/1.4025988]

Keywords: anomaly detection, rotorcraft instability, probabilistic finite state automata, damping estimation

1 Introduction

Rotorcraft are complex dynamical systems involving many degrees of freedom, strong couplings between structural dynamics and aerodynamics (i.e., aeroelasticity), and a variety of linear and nonlinear dynamics that are susceptible to instability. Ensuring dynamic stability over the entire flight envelope is a challenging task in the sense that rotorcraft dynamics are difficult to predict over a wide range of operating conditions. For example, unstable vibratory oscillations in the rotor system may lead to component failures, while low-frequency instabilities due to the coupled pilot-vehicle dynamics may cause loss of control. There are numerous

other examples of unstable dynamic behavior, which are prevalent in rotorcraft systems. Some of the common sources of instability that characterize rotorcraft dynamics are delineated below:

- (1) *Rotor system instability*: The pitch and lag motions of a rotorcraft may change from stable periodic to unstable limit cycling as an equilibrium point becomes unstable at large-torque flight conditions [1].
- (2) *Ground resonance instability*: A rotorcraft may exhibit violent fuselage roll oscillations, while resting on the ground with the rotor spinning [2].
- (3) *Hover flutter instability*: This instability may occur due to the coalescence of blade pitch and flap modes [3].
- (4) *Rotor stall flutter instability*: This is another form of flutter, where limit-cycle oscillations of pitch-flap may occur as the rotor state progresses past the aerodynamic stall boundary [4].
- (5) *Rotor-body coupling instability*: This instability results from undesired interactions between the fuselage dynamics, rotor dynamics, and possibly the flight control system specifically due to the lightly damped lag mode [5].
- (6) *Pilot-induced oscillations*: These oscillations may occur in slung loads with a large load-to-mass ratio due to unstable interactions between flight dynamics and pilot-induced feedback compensation [6].

Stability characteristics for rotorcraft are dependent upon a variety of structural and aerodynamic properties, such as aircraft mass distribution, flight or test condition as well as the pilot's actions. Developing accurate models of these complex dynamical phenomena is extremely difficult, and such models are always subjected to significant uncertainties, especially in the extreme regions of the flight envelope. It is not always practical to apply model-based stability analyses (e.g., Lyapunov stability theory) to these complex rotorcraft systems, which cannot be accurately represented by simple analytical models. At the same time, the rotorcraft control system must ensure that the instabilities do not become symptomatic within the flight envelope. Therefore, stability of rotorcraft dynamics needs to be verified through different types of testing (e.g., rotor whirl testing, wind tunnel testing, and flight testing). Such tests are expensive and extraction of relevant data is nontrivial due to, for example, rotating components and poor SNR of collected data.

Andrews and Wong [7] have reported a comprehensive review of the popularly used methods to perform stability estimation in rotorcraft systems. Prony's method (that relies on multifrequency curve-fitting) was extensively used for estimation of damping ratios in the 1990's. Although Prony's method is suitable for design validation and offline testing, it has two major drawbacks, namely, low computational efficiency and the requirement for a dwell input, which make the implementation difficult for real-time stability monitoring. Subspace identification methods have gained popularity over the last decade [8], which are based on the assumption that the dynamical system is linear time-invariant; however, in general, rotorcraft dynamics are nonlinear in nature as explained earlier.

A major challenge in feedback control of rotorcraft system dynamics is extraction of meaningful information from the acquired sensor data, which suffers from low SNR of the acquired data. This is so because the meaningful dynamical information, imbedded in the small-amplitude signals, could be intermittent. In addition, there are dominant disturbances at rotor speed harmonics that often provide only limited information on stability characteristics. For example, in the forward flight of a rotorcraft, a series of harmonics occur at integer multiples of the rotor speed and these harmonics dominate the signals generated from sensors [7]. This problem was recognized early in the development of rotorcraft control systems; previous attempts to remove the harmonics from sensor data, which have included the usage of fast Fourier transform, Kalman filtering, notch filters, and averaging over revolutions [9], have not been very successful. Thus, filtering methods based upon time-frequency transforms have become a critical

Contributed by the Dynamic Systems Division of ASME for publication in the JOURNAL OF DYNAMIC SYSTEMS, MEASUREMENT, AND CONTROL. Manuscript received March 6, 2013; final manuscript received November 5, 2013; published online January 8, 2014. Assoc. Editor: Jiong Tang.

aspect of signal pre-processing and one such method, namely, wavelet packet (WP) decomposition [10] is adopted in this paper.

With the objective of detecting and quantifying instabilities in rotorcraft dynamics, this paper proposes a dynamic data-driven approach as an extension of the authors' recently reported work [11]. The underlying theory is built upon the concept of symbolic dynamic filtering (SDF) [12] that circumvents some of the difficulties and shortcomings in model-based analysis. In previous publications [13–16], SDF has been demonstrated to be an effective tool to detect anomalies in a variety of nonlinear systems. In essence, the expected role of the proposed dynamic data-driven method is to detect and estimate changes in rotorcraft system stability relative to a nominal baseline that serves as a reference. The dynamic data-driven method is developed to predict relative stability from a sample data set with known stability properties, and is tested to determine whether it can generalize the predictions across unknown data sets; it does not require a computation-intensive analytical representation of the system dynamics. The stability monitoring algorithm, developed in this paper, is potentially capable of real-time monitoring and identification of incipient instabilities (e.g., those due to lightly damped modes) in rotorcraft systems.

The paper is organized in four sections including the present section. The core concept of the proposed method is outlined in Sec. 2, while the details of the theoretical background are reported in the cited references. Section 3 presents the results based on numerical simulations of on a multi-degree-of-freedom model that is a simplified representation of the aeroelastic dynamics of a helicopter rotor. Section 4 concludes the paper along with recommendations for future research.

2 SDF

Symbolic time series analysis [17] is a data-driven tool that is built upon the principle of symbolic dynamics, and it has been used for signal characterization in dynamical systems. SDF [12,13] is an extension of symbolic time series analysis, where the time series data are preprocessed by transformation in the time-frequency domain. The processed data are symbolized for construction of probabilistic finite state automaton (PFSA) from the symbol sequences. Diverse applications of SDF for anomaly detection and pattern recognition have been reported in the scientific literature (e.g., Ref. [16]). The concept of SDF has been used in this paper for construction of an instability measure in rotorcraft dynamics. While the details of SDF have been presented in previous publications (e.g., Refs. [12,13]), this section succinctly outlines the pertinent concepts of SDF in the following two subsections.

2.1 Wavelet Packet Preprocessing. The sensor time series data are preprocessed by WP decomposition [10] that is a generalization of multiresolution approximation (MRA) in wavelet analysis [18]. The tree structure of WP is constructed conceptually similar to that of MRA, which produces an orthonormal time-frequency decomposition of the analyzed signal. While the frequency bands of MRA bear dyadic (i.e., powers of 2) relationships with each other, WP may not retain the orthogonality property of the wavelet bases in order to achieve finer frequency granularity and flexibility in the mode of signal decomposition. For example, a part of the signal can be left unchanged if it is not desired to be decomposed; similarly, a part of the frequency spectrum can be filtered out by setting the associated coefficients to zero.

The discrete wavelet basis function of Meyer (i.e., “dmey” in the MATLAB toolbox [19]) has been adopted in the MRA; the rationale for adopting the Meyer wavelet basis function is similarity of the shapes of its wavelet (ψ) and scaling (ϕ) functions (see Fig. 1) with those of the approximately sinusoidal waveforms of sensor time series. The results of WP decomposition show that the harmonics generated at the sampling frequency of 2^J appear as constant coefficients at level J of MRA. Therefore, removing the wavelet coefficients at level J would significantly eliminate the spurious harmonics, and nonsynchronous signals that have energy

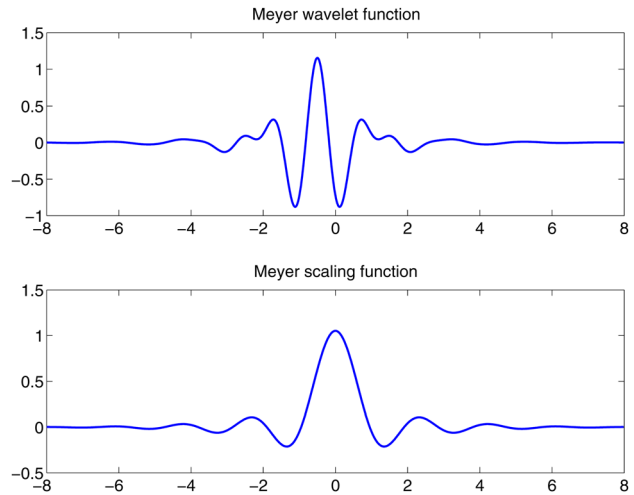


Fig. 1 Typical wavelet and scaling functions of Meyer basis

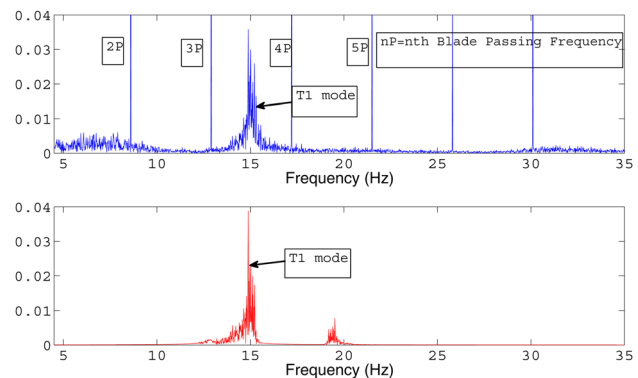


Fig. 2 Effects of wavelet packet preprocessing

at the harmonic frequencies would not be removed [20]. Figure 2 illustrates how the undesirable harmonics are largely filtered out when the signal is acquired at 1024 samples/revolution (i.e., at level $J = \log_2(1024) = 10$). It is also seen that the asynchronous signals are retained even at the harmonic frequencies. However, removal of the synchronous harmonics may still leave behind undesirable signals with nonnegligible energy in the vicinity of the harmonic frequencies due to sampling at a nonzero phase. Since the resulting near-harmonic energy may cause very low frequency oscillations in the WP coefficients, a low-order high-pass filter was constructed to serve the purpose of dc-blocking.

2.2 Symbolization of the Filtered Time Series. SDF encodes the behavior of (possibly nonlinear) dynamical systems from the filtered time series by symbolization and state machine construction. This is followed by computation of the state probability vectors (or morph matrices) that are representatives of the evolving statistical characteristics of the dynamical system. Symbolization is achieved by partitioning the filtered time series data into a mutually exclusive and exhaustive set of finitely many cells. In this paper, maximum-entropy partitioning [13] has been adopted to construct the symbol alphabet Σ and to generate symbol sequences, where the information-rich regions of the data set are partitioned finer and those with sparse information are partitioned coarser to maximize the Shannon entropy of the generated symbol sequence from the reference data set. As seen at the upper left hand corner plot of Fig. 3, each cell is labeled by a unique symbol and let Σ denote the alphabet of all these symbols. The cell, visited by the time response plot takes a symbol value from Σ . For example, having $\Sigma = \{\alpha, \beta, \gamma, \delta\}$ in Fig. 3, a filtered time-series

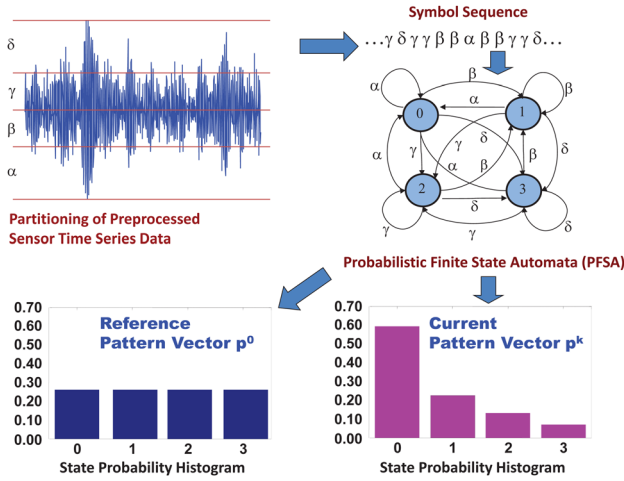


Fig. 3 Concept of SDF

$x_0x_1x_2\dots$ generates a sequence of symbols in the symbol space as: $s_0s_1s_2\dots$, where each $s_i, i = 0, 1, 2, \dots$, takes a symbol value from the alphabet Σ . This mapping is called symbolic dynamics as it attributes a (physically admissible) symbol sequence to the dynamical system starting from an initial state. For example, see the symbol sequence at the top right hand corner of Fig. 3.

The core assumption in the SDF analysis for construction of PFSA from symbol sequences is that the symbolic process under both nominal and off-nominal conditions can be approximated as a Markov chain of order D , called the D -Markov machine, where D is a positive integer. While the details of the D -Markov machine construction are given in Refs. [12,13,21], the pertinent definitions and their implications are presented below.

DEFINITION 2.1: (DFSA) A deterministic finite state automaton (DFSA) is a 3-tuple $G = (\Sigma, Q, \delta)$ where:

- (1) Σ is a nonempty finite set, called the symbol alphabet, with cardinality $|\Sigma| < \infty$;
- (2) Q is a nonempty finite set, called the set of states, with cardinality $|Q| < \infty$;
- (3) $\delta : Q \times \Sigma \rightarrow Q$ is the state transition map;

and Σ^* is the collection of all finite-length strings with symbols from Σ including the (zero-length) empty string ϵ , i.e., $|\epsilon| = 0$.

Remark 2.1. It is noted that Definition 2.1 does not make use of an initial state, because the purpose here is to work in a statistically stationary setting, where no initial state is required as explained by Adenis et al. [21].

DEFINITION 2.2. A PFSA is constructed upon a DFSA $G = (\Sigma, Q, \delta)$ as a pair $K = (G, \pi)$, i.e., the PFSA K is a 4-tuple $K = (\Sigma, Q, \delta, \pi)$, where:

- (1) Σ, Q , and δ are the same as in Definition 2.1;
- (2) $\pi : Q \times \Sigma \rightarrow [0, 1]$ is the probability morph function that satisfies the condition $\sum_{\sigma \in \Sigma} \pi(q, \sigma) = 1 \forall q \in Q$. Denoting π_{ij} as the probability of occurrence of a symbol $\sigma_j \in \Sigma$ at the state $q_i \in Q$, the $(|Q| \times |\Sigma|)$ probability morph matrix is obtained as $\Pi = [\pi_{ij}]$.

DEFINITION 2.3. (D -Markov) A D -Markov machine [12] is a PFSA in which each state is represented by a finite history of D symbols as defined by:

- D is the depth of the Markov machine;
- Q is the finite set of states with cardinality $|Q| \leq |\Sigma|^D$, i.e., the states are represented by equivalence classes of symbol strings of maximum length D where each symbol belongs to the alphabet Σ ;

- $\delta : Q \times \Sigma \rightarrow Q$ is the state transition map that satisfies the following condition if $|Q| = |\Sigma|^D$: There exist $\alpha, \beta \in \Sigma$ and $s \in \Sigma^*$ such that $\delta(\alpha s, \beta) = s\beta$ and $\alpha s, s\beta \in Q$.

Remark 2.2. It follows from Definition 2.3 that a D -Markov chain is a statistically (quasi-)stationary stochastic process $S = \dots s_{-1}s_0s_1\dots$, where the probability of occurrence of a new symbol depends only on the last D symbols, i.e., $P[s_n|s_{n-1}\dots s_{n-D}\dots s_0] = P[s_n|s_{n-1}\dots s_{n-D}]$.

The construction of a D -Markov machine is based on: (i) state splitting that generates symbol blocks of different lengths according to their relative importance; and (ii) state merging that assimilates histories from symbol blocks leading to the same symbolic behavior. Words of length D on a symbol sequence are treated as the states of the D -Markov machine before any state-merging is executed. Thus, on an alphabet Σ , the total number of possible states becomes less than or equal to $|\Sigma|^D$; and operations of state merging may significantly reduce the number of states [22].

Following Fig. 3, the filtered time series at a given epoch t^k may now be used to compute the quasi-stationary probability morph matrix Π^k (see Definition 2.2) that, in conjunction with the state transition map δ (see Definition 2.1), is used to construct the $(|Q| \times |Q|)$ stochastic quasi-stationary irreducible state-transition matrix as: $\mathbf{P}^k \triangleq [\mathbf{P}_{ij}^k]$, where \mathbf{P}_{ij}^k is the probability of transition from state q_i to state q_j based on time series at epoch t^k . The corresponding state probability vector is obtained as: $\mathbf{p}^k \triangleq [p_1^k, \dots, p_{|Q|}^k]$, where p_j^k is the quasi-stationary probability of occupying the state $q_j \in Q$ at epoch t^k , as the (sum-normalized) left eigenvector of \mathbf{P}^k corresponding to its (unique) unity eigenvalue.

Let the quasi-stationary statistics of the time series at the epoch t^k , represented by the state transition probability matrix \mathbf{P}^k , change to \mathbf{P}^ℓ at another epoch t^ℓ . Accordingly, the state probability vector \mathbf{p}^k changes to \mathbf{p}^ℓ ; thus, \mathbf{p}^k can be treated as a pattern vector that is postulated to have the imbedded information on stability of the dynamical system at the epoch t^k . Another viable candidate for the pattern at an epoch t^k is the probability morph matrix Π^k (see Definition 2.2). It is noted that Π^k carries more information than the respective \mathbf{p}^k at the expense of higher dimensionality. Two histograms at the bottom of Fig. 3 exemplify the pattern vectors \mathbf{p}^0 and \mathbf{p}^k .

Now, we introduce the concept of instability measure of a dynamical system at an epoch t^k relative to its nominal condition at an epoch t^0 as a (scalar non-negative) distance between the patterns generated from the respective quasi-stationary time series data.

DEFINITION 2.4. (Instability Measure) The instability measure of a dynamical system at an epoch t^k is obtained relative to its nominal condition at an epoch t^0 as the distance $d(\mathbf{p}^k, \mathbf{p}^0)$ [resp., $d(\Pi^k, \Pi^0)$] of the current pattern vector \mathbf{p}^k [resp., Π^k] from the reference pattern vector \mathbf{p}^0 [resp., Π^0] at the nominal condition denoted by the superscript '0'. In this paper, instability measure of rotorcraft dynamics at an epoch t^k is defined to be the Euclidean distance between \mathbf{p}^k and \mathbf{p}^0 .

$$\mu^k \triangleq \sqrt{(\mathbf{p}^k - \mathbf{p}^0)^T (\mathbf{p}^k - \mathbf{p}^0)} \quad (1)$$

3 Algorithm Validation on a Simulation Test Bed

This section presents validation of the proposed algorithm on a simulation test bed for detection and identification of instabilities associated with the aeroelastic modes of helicopter rotor blades. The simulation test bed is constructed on a multi-degree-of-freedom model that is a simplified representation of the aeroelastic dynamics of a helicopter rotor. In its nominal linear configuration, the simulation model consists of multiple decoupled second-order systems (i.e., modes) with each mode having its respective damping parameter and natural frequency. Each mode is simultaneously excited by a combination of additive noise and sinusoidal inputs with frequencies at integer

Table 1 Details of linear multidegree of freedom model

Description of modes $i = 1, \dots, N_m = 6$	Frequency $\frac{\omega_i}{2\pi}$ (Hz)	Damping parameter $100\zeta_i$ (percent critical)
Rigid chordwise (C1)	2	16
Rigid edgewise (F1)	7	26
Rigid torsion (T1)	15	10–0.5
1st Elastic flatwise (F2)	20	17
2nd Elastic flatwise (F3)	31	5
2nd Elastic chordwise (C2)	33	13

multiples of a notional blade passing frequency P (e.g., $P = 4.3$ Hz in a typical helicopter rotor). The simulation model generates sensor outputs with a frequency spectrum that is similar to that of signals obtained from sensors on an instrumented rotor blade and also to those produced by comprehensive aeroelastic simulation of typical rotor systems [23]. The structure of the governing equations of the displacements x_i for the (decoupled) modes, $i = 1, \dots, N_m$, of the nominal linear model is presented below.

$$\ddot{x}_i(t) + 2\zeta_i\omega_i\dot{x}_i(t) + \omega_i^2x_i(t) = \sum_{j=1}^{N_m+1} a_j \sin(\Omega_j t) + W_t \quad (2)$$

where ζ_i and ω_i are, respectively, the damping parameter and natural frequency of the mode $i = 1, \dots, N_m$; the excitation frequencies are $\Omega_j = 2\pi jP, j = 1, \dots, N_m + 1$; individual excitation amplitudes $a_j \in [0, 1]$; and the additive noise W_t . The time series data are generated from the sensor output that is modeled as: $y(t) = \sum_{j=1}^{N_m} w_j x_j(t)$ with weights $w_j \in [0, 1]$.

For the nominal model in the simulation test bed, the parameters are selected as: blade passing frequency $P = 4.3$ Hz; the number of modes $N_m = 6$; excitation amplitude $a_j = 1\forall j$; white Gaussian noise $W_t \sim \mathcal{N}(0, 1)$; and output weights $w_j = 1\forall j$. Table 1 presents a

description of the six modes ($N_m = 6$) and lists numerical values of the modal parameters ζ_i and ω_i that are generated based on the results reported in a recent publication [7].

Validation tests have been conducted on sensor outputs, generated from the simulation test bed, that include measurements of the blade angles (i.e., pitch, lag, flap), the lag damper force, and structural forces and moments at locations along the length of the blade [7]. The sensor signals, under rotorcraft motion with forward velocity, are dominated by (input excitation) harmonics located at integer multiples of the rotor angular frequency, i.e., at $(1P, 2P, 3P, \dots)$. However, since these signals represent harmonic forces on the rotor system due to unsteady loading on the blades in the forward flight, they do not provide any significant information on relative stability of the dynamic modes of the rotor system. Nevertheless, it is a challenging task to analyze the embedded information on the dynamic modes, due to the presence of strong harmonics in the sensor data.

For stability analysis, the signal contents of the harmonics centered around the modal frequency are filtered out by the WP preprocessing. For example, the signal pertaining to the rigid torsion (T1) mode at 15 Hz is extracted from the time series, as seen in Fig. 2; the modal frequency is located between the three per rev harmonic at $3P = 12.9$ Hz and the four per rev harmonic at $4P = 17.2$ Hz.

Now, the task at hand is to validate the SDF-based algorithm to detect and estimate the degradation of stability phenomena as the damping parameter is monotonically decreased. This is accomplished first by generating blocks of time series data for a number of different test samples on the simulation test bed by using the linear model (see Eq. (2)). In the (simulated) statistical tests, each test sample signifies a (hypothetical) helicopter rotor that is represented by a fixed seed number in the random number generator. For each seed number, a single profile of instability measure μ is constructed as the damping parameter ζ (see Eq. (2)) is varied from 10 to 0.5 percent of the critical damping parameter (see Table 1); the reference condition is at $\zeta = 10$ at which $\mu = 0$ (see Eq. (1)). An envelope of statistical confidence interval is

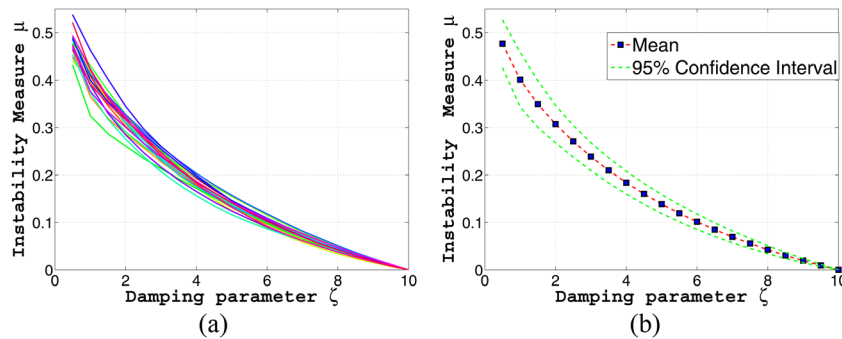


Fig. 4 Profile of Instability Measure for the T1 mode at 15 Hz (a) ensemble of plots with ζ in. % and (b) confidence interval with ζ in. %

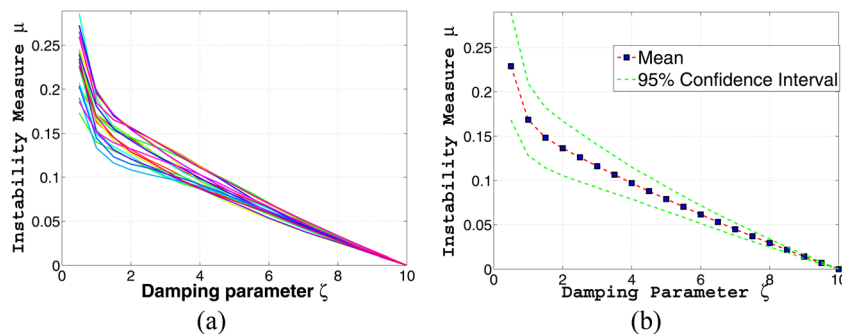


Fig. 5 Profile of Instability Measure for the T1 mode at 17 Hz (a) ensemble of plots with ζ in. % and (b) confidence interval with ζ in. %

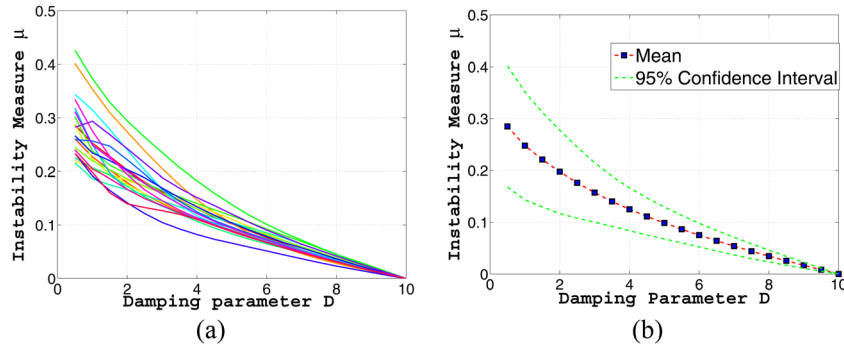


Fig. 6 Profile of *Instability Measure* with the exponent $\epsilon = 0.5$ (see Eq. (3)) (a) ensemble of plots with D in. % and (b) confidence interval with D in. %

constructed from the ensemble of $\zeta - \mu$ profiles. Figure 4(a) shows an ensemble of $\zeta - \mu$ profiles for the T1-mode at 15 Hz in the linear model of Eq. (2), where each profile (i.e., each simulated rotor represented by a seed of the random number generator) exhibits a monotonically decreasing correlation between the damping parameter ζ and the instability measure μ . Figure 4(b) exhibits the mean value and the envelope of 95% confidence of the $\zeta - \mu$ profiles, which also show a smooth monotonic trend.

Next the effects of moving a dynamic mode close to a harmonic forcing frequency are investigated. The simulated T1 mode was originally placed at 15 Hz; it is now moved to 17 Hz, which is very close to the fourth blade passing frequency $4P = 17.2$ Hz. Figure 5(a) shows the resulting profiles of *Instability Measure* μ as the damping parameter ζ is varied. Similar to what is seen in Fig. 4(a), a monotonic decrease of *Instability Measure* μ is observed with increase in the damping parameter ζ , although the envelope of confidence interval in Fig. 5(a) is significantly wider than that in Fig. 4(a) and the range of the *Instability Measure* μ in Figs. 5(a) and 5(b) is approximately half of that in Figs. 4(a) and 4(b). As reported by Andrews and Wong [7], it is difficult to estimate, solely based on sensor outputs, the damping parameter of a mode that is close to a blade passing frequency. Although μ is not as sensitive to ζ in Fig. 5(b) as it is in Fig. 4(b), there still exists a strong monotonic correlation between ζ and μ .

Investigation of system nonlinearity effects is a challenge in rotorcraft system stability analysis as the system nonlinearity. Since the model used in the above case studies is linear, efficacy of the stability monitoring algorithm is further tested on nonlinear models. To this end, the linear structure of the rotor dynamic model in Eq. (2) is reconfigured to have a nonlinearity by modifying the damping parameters in one or more modes. In the nonlinear model, the damping parameter ζ_i in the i th mode (see Eq. (2)) is replaced as follows:

$$D_i |\dot{x}_i(t)|^\epsilon \rightarrow \zeta_i \quad (3)$$

where the nonlinear damping parameter $D_i \in [0.5, 10] \times 10^{-2}$ and the exponent $\epsilon \in [0, 1]$.

Similar to the above two cases dealing with the linear model, simulated sensor data have been generated from the nonlinear model by introducing velocity dependence in the damping parameter D (see Eq. (3)) associated with the T1 mode at 15 Hz. Figures 6(a) and 6(b) show the performance of the stability monitoring algorithm for a nonlinear model with the exponent $\epsilon = 0.5$ in Eq. (3), where relatively large spreads in the instability measure are observed for low damping. A possible reason for this behavior is rapidly varying dissipation in the system model due to fluctuations in the velocity term.

4 Conclusions

This paper presents the development of a dynamic data-driven method for quantification of instability measure in different oper-

ating modes of rotorcraft systems. The core concept is built upon SDF [12] of sensor time series data that are filtered by wavelet-packet-based preprocessing [10,20]. The proposed method has the potential to serve as a critical safety tool for stability monitoring of rotorcraft flight dynamics and possibly could be used as an input to the rotorcraft control system for vehicle stability enhancement. However, the work reported in this paper is a preliminary analysis and would require significant analytical and experimental research before its real-life application. Some of the key research issues are delineated as topics of future research:

- Investigation of appropriate wavelet basis for signal preprocessing [18].
- Enhancement of the SDF algorithm by using the tools of state splitting and state merging [22].
- Statistical estimation of the instability measure μ by taking advantage of the data history [24].
- Comparison of the proposed method of instability estimation with standard tools used in the dynamics and control literature.
- Validation of the proposed method on a high-fidelity simulation test bed (e.g., rotorcraft comprehensive analysis system (RCAS) [23]) for different operational scenarios.

Acknowledgment

The authors acknowledge the benefits of discussion with Dr. Shashi Phoha at Applied Research Laboratory of Pennsylvania State University.

This work was supported in part by the U.S. Army Aviation and Missile Research, Development, and Engineering Center (AMRDEC) under Technology Investment Agreement W911W6-05-2-0003, by the U.S. Air Force Office of Scientific Research (AFOSR) under Grant No. FA9550-12-1-0270, and by the U.S. Army Research Laboratory and the U.S. Army Research Office under Grant No. W911NF-07-1-0376.

References

- [1] Friedmann, P., and Tong, P., 1972, "Dynamic Nonlinear Elastic Stability of Helicopter Rotor Blades in Hover and in Forward Flight," Aeroelastic and Structures Research Laboratory, Department of Aeronautics and Astronautics, Massachusetts Institute of Technology, Cambridge, MA 02139.
- [2] Kunz, D. L., 2002, "Nonlinear Analysis of Helicopter Ground Resonance," *Nonlinear Anal.: Real World Appl.*, 3(3), pp. 383–395.
- [3] Johnson, W., 2003, "A Comprehensive Analytical Model of Rotorcraft Aerodynamics and Dynamics. Part 1: Analysis Development," NASA Ames Research Center, Moffet Field, CA.
- [4] Crimi, P., 1973, "Analysis of Stall Flutter of a Helicopter Rotor Blade," National Aeronautics and Space Administration, Washington, D.C. 20546.
- [5] Fletcher, J. W., Lusardi, J., Mansur, M. H., Moralez, E., Robinson, D. E., Arterburn, D. R., Cherepinsky, I., Driscoll, J., Morse, C. S., and Kalinowski, K.F., 2008, "UH-60M Upgrade Fly-By-Wire Flight Control Risk Reduction

- Using the RASCAL JUH-60A in-Flight Simulator,” Proceedings of the American Helicopter Society 64th Annual Forum, Montreal, Canada.
- [6] Lusardi, J. A., 2010, “Development of External Load Handling Qualities Criteria for Rotorcraft,” Proceedings of the American Helicopter Society 66th Annual Forum, Phoenix, AZ.
- [7] Andrews, J., and Wong, J., 2012, “Real-Time Extraction of Rotor Modal Information for Stability Monitoring and Correlation,” Proceedings of the American Helicopter Society Future Vertical Lift Aircraft Design Conference, San Francisco, CA.
- [8] van Overschee, P., and Moor, B. D., 1996, *Subspace Identification for Linear Systems: Theory, Implementation and Applications*, Kluwer Academic Publishers, Dordrecht, The Netherlands.
- [9] Goodwin, G., Evans, R., Leal, R., and Feik, R., 1986, “Sinusoidal Disturbance Rejection With Application to Helicopter Flight Data Estimation,” *IEEE Trans. Acoust., Speech, Signal Process.*, **34**(3), pp. 479–484.
- [10] Coifman, R. R., Meyer, Y., and Wickerhauser, M. V., 1992, “Wavelet Analysis and Signal Processing,” *Wavelets and Their Applications*, Ruskai, M. B., Beylkin, G., Coifman, R. R., Daubechies, I., Mallat, Meyer, Y., and Raphael, L., eds. Jones and Bartlett, Boston, MA, pp. 153–178.
- [11] Sonti, S., Keller, E., Horn, J., and Ray, A., 2013, “Identification of Instabilities in Rotorcraft Systems,” Proceedings of Dynamic Systems and Control Conference, Stanford, CA.
- [12] Ray, A., 2004, “Symbolic Dynamic Analysis of Complex Systems for Anomaly Detection,” *Signal Process.*, **84**(7), pp. 1115–1130.
- [13] Rajagopalan, V., and Ray, A., 2006, “Symbolic Time Series Analysis Via Wavelet-Based Partitioning,” *Signal Process.*, **86**(11), pp. 3309–3320.
- [14] Gupta, S., Ray, A., and Keller E., 2007, “Symbolic Time Series Analysis of Ultrasonic Data for Early Detection of Fatigue Damage,” *Mech. Syst. Signal Process.*, **21**(2), pp. 866–884.
- [15] Chakraborty, S., Keller, E., Talley, J., Srivastav, A., Ray, A., and Kim, S., 2009, “Void Fraction Measurement in Two-Phase Processes Via Symbolic Dynamic Filtering of Ultrasonic Signals,” *Meas. Sci. Technol.*, **20**(2), p. 023001.
- [16] Mallapragada, G., Ray, A., and Jin, X., 2012, “Symbolic Dynamic Filtering and Language Measure for Behavior Identification of Mobile Robots,” *IEEE Trans. Syst., Man, Cybern., Part B: Cybern.*, **42**(3), pp. 647–659.
- [17] Daw, C. S., Finney, C. E. A., and Tracy, E. R., 2003, “A Review of Symbolic Analysis of Experimental Data,” *Rev. Sci. Instrum.*, **74**(2), pp. 915–930.
- [18] Mallat, S., 2009, *A Wavelet Tour of Signal Processing: The Sparse Way*, 3rd ed., Academic, Amsterdam, The Netherlands.
- [19] Zhao, J., 2011, *Wavelet Toolbox*, Mathworks Inc., Natick, MA.
- [20] Xu, L., 2005, “Cancellation of Harmonic Interference by Baseline Shifting of Wavelet Packet Decomposition Coefficients,” *IEEE Trans. Acoust., Speech, Signal Process.*, **53**(1), pp. 222–230.
- [21] Adenis, P., Wen, Y., and Ray, A., 2012, “An Inner Product Space on Irreducible and Synchronizable Probabilistic Finite State Automata,” *Math. Control, Signals, Syst.*, **23**(4), pp. 281–310.
- [22] Adenis, P., Mukherjee, K., and Ray, A., 2011, “State Splitting and State Merging in Probabilistic Finite State Automata,” Proceedings of the American Control Conference, San Francisco, CA.
- [23] Structural Rotorcraft Comprehensive Analysis System (RCAS) Theory Manual, Version 2.0., 2003, US Army Aviation and Missile Command, Moffett Field, CA.
- [24] Singh, D., Gupta, S., and Ray, A., 2012, “Online Recursive Estimation of Remaining Life Using Ultrasonic Measurements,” *Struct. Health Monit.*, **11**(4), pp. 413–421.